Chemical Sensors and Electronic Noses Based on 1-D Metal Oxide Nanostructures

Po-Chiang Chen, Guozhen Shen, and Chongwu Zhou, *Member, IEEE*

(Invited Paper)

***Abstract*—The detection of chemicals such as industrial gases and chemical warfare agents is important to human health and safety. Thus, the development of chemical sensors with high sensitivity, high selectivity, and rapid detection is essential and could impact human beings in significant ways. 1-D metal oxide nanostructures with unique geometric and physical properties have been demonstrated to be important candidates as building blocks for chemical sensing applications. Chemical sensors composed of a wide range of pristine 1-D metal oxide nanostructures, such as In_2O_3, SnO_2, ZnO, TiO_2, and CuO, have been fabricated, and exhibited very good sensitivity in the detection of important industrial gases, chemical warfare agents, and human breath. In this review, we provide an overview of this chemical sensing field. Various key elements of the topics will be reviewed, including 1-D metal oxide nanostructure synthesis, electronic properties of nanowire-based FETs, and their chemical sensing behaviors. In addition, this paper provides a review of the recent development of electronic nose systems based on metal oxide nanowires, which indicate great potential for the improvement of sensing selectivity.**

***Index Terms*—Electronic noses, metal oxide nanowire synthesis, nanowire chemical sensors, nanowire FETs.**

I. Introduction

CHEMICAL sensors such as conductive polymer sensors [1], [2], surface acoustic wave (SAW) sensors [3], [4], metal oxide sensors [5], [6], and microcantilever sensors [7] have important applications in the area of environmental monitoring, public security, automotive application, and medical diagnosis. Over the past few decades, researchers and engineers have dedicated their effort to develop both materials and sensors with the characteristics of high sensitivity, good selectivity, and reliability. Till now, most commercial sensors were based on pristine or doped metal oxides due to their compatibility with high temperature operation [8] and great sensitivity, when compared with other active materials. Sensors and electronic noses based on metal oxide thin-film [9], [10] materials have potential for many applications, including the National Aeronautics and Space Administration (NASA) space shuttle programs [11].

In 1998, Morales and Lieber demonstrated the synthesis of single-crystalline Si nanowires using the laser ablation method [12]. Inspired by this work, enormous progress has been made in the synthesis of single-crystalline 1-D nanostructured materials including metals [13]–[16], III–V semiconductors [17]–[20], IV–VI semiconductors [21]–[24], and metal oxides [25]–[30]. The achievements in the synthesis of nanostructured materials enabled scientists to explore the physical, chemical, and electronic properties for various applications in the field of nanoelectronics [31]–[35], nanooptics [36]–[38], energy conversion [39]–[41], and chemical sensing [42]–[48].

With large surface-to-volume ratios and Debye length comparable to their small size, these 1-D nanostructures have already displayed superior sensitivity to surface chemical processes [49]–[54]. For example, Comini *et al.* [55] reported the first SnO_2 nanobelt chemical sensor in the detection of CO, ethanol, and NO_2 at elevated temperatures (300–400 °C). The reported detection limit of NO_2 was 0.5 ppm in the synthetic air. In the sense of practical applications, both sensitivity and selectivity are important topics to the chemical sensing community. By using chemical coating [56], [57] or nanoparticle decoration [58]–[60], both device sensitivity and selectivity can be improved. In addition, the electronic nose technique [61] is one of the approaches to solve the selectivity problem. We note that both nanowires and conventional films based on nanostructures can offer good chemical sensing performance; however, nanowires can offer certain advantages such as precise diameter control, easy integration into transistor configuration, and single-crystalline material quality.

This paper is restricted primarily to chemical sensors and electronic nose systems based on 1-D semiconducting oxide nanostructures, including nanobelts, nanoribbons, and nanowires. Section II introduces the synthesis of 1-D metal oxide nanostructures, including vapor phase growth and a laser ablation method. Section III discusses the electronic properties of metal oxide nanowires. In Section IV, chemical sensing based on different 1-D metal oxides including In_2O_3, ZnO, SnO_2, V_2O_5, CuO, TiO_2, and WO_3 will be discussed. The concept of electronic noses and recent achievements will be studied in Section V. Finally, an outlook on other possible and new applications of 1-D metal oxide nanostructure chemical sensor is presented in Section VI.

II. Synthesis of 1-D metal Oxide Nanostructures

Over the past decades, a variety of approaches including electrochemical deposition [66], hydrothermal process [25], vapor phase growth [26], and solution phase growth [27], [28] have been developed to obtain bulk-quantity and high-quality 1-D semiconducting nanostructured materials (see Table I). Among

Manuscript received June 2, 2008; accepted September 5, 2008. First published September 26, 2008; current version published December 24, 2008. The review of this paper was arranged by Associate Editor J. Li.

The authors are with the Ming-Hsieh Department of Electrical Engineering, University of Southern California, Los Angeles, CA 90089 USA (e-mail: chongwuz@usc.edu).

Color versions of one or more of the figures in this paper are available online at http://ieeexplore.ieee.org.

Digital Object Identifier 10.1109/TNANO.2008.2006273

TABLE I
SYNTHETIC METHODS DEVELOPED FOR THE SYNTHESIS OF 1-D METAL OXIDE NANOMATERIALS [62]–[65]

Synthetic Methods		Products	Advantages/Disadvantages
Vapor phase synthesis (Thermal evaporation, CVD, Laser ablation, MOCVD)	VLS growth	ZnO, SnO_2, In_2O_3, Fe_2O_3, MgO NWs, *etc.*	*Advantages*: 1. Typically produce high quality single-crystalline nanowires with easy control over the diameter and length; 2. Capable of producing nanowires on a large scale. *Disadvantages*: 1. Need high temperature; 2. complicated procedures are needed in some methods.
	VS growth	ZnO, SnO_2, In_2O_3, Cu_2O, WO_3, Co_3O_4, V_2O_5, MgO, Ga_2O_3 NWs, *etc.*	
Solution phase synthesis	Template-free growth	ZnO, SnO_2, V_2O_5, MnO_2 NWs, *etc.*	*Advantages*: Only need ambient temperature with reduced fabrication complexity and cost. *Disadvantages*: 1. Typically difficult to control the diameter of nanowires; 2. Template-assisted method usually produces poly-crystalline nanowires.
	Template-assisted growth	ZnO, TiO_2, SnO_2 NWs, *etc.*	
Other methods (electrospinning, *etc.*)		TiO_2, ZnO, SnO_2 NWs, *etc.*	It usually requires complicated procedure and is difficult to control diameters.

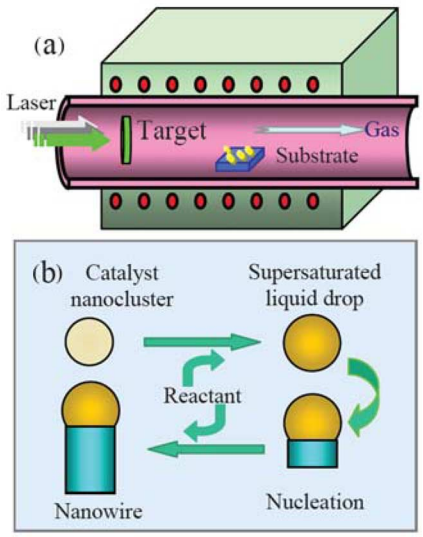

Fig. 1. (a) Schematic diagram of a laser-assisted chemical vapor deposition setup. (b) Illustration of the VLS mechanism.

these methods, the vapor phase growth, governed by the vapor–liquid–solid (VLS) and vapor–solid (VS) mechanisms, is one of the most promising methods since it provides an easy and cost-efficient way to produce numerous single-crystalline 1-D nanomaterials with precise diameter control down to 10 nm, and thus, enables the production of nanowires on a large scale.

The laser-assisted chemical vapor deposition system is one of the vapor phase growth methods, and a schematic diagram is shown in Fig. 1(a). Detailed experimental setup can be found in the literature [67]. Here, we would like to use In_2O_3 nanowire as an example. Briefly, Si/SiO_2 substrates coated with gold clusters were placed into a quartz tube at the downstream end of a furnace and the gold clusters were used as the catalysts for the In_2O_3 nanowires growth. An InAs target is placed at the upper stream of the furnace and laser ablated to supply the In vapor. The approach is based on the VLS growth mechanism, where the In vapor first diffuses into the gold catalytic particles and forms In/Au liquid drops, as shown in Fig. 1(b). Continued addition of In into the In/Au drops brings the alloy beyond supersaturation and leads to the nucleation of In, which reacts with the ambient oxygen and yields In_2O_3. Further supply of In vapor feeds the In_2O_3 growth, and eventually the diameter of the In_2O_3 nanowire is directly linked to the catalytic particle size.

After material synthesis, it is necessary to check the material quality by SEM, X-ray diffractometer (XRD), transmitted electron microscopy (TEM), and selected area electron diffraction (SAED), which will be discussed in the following sections.

A. Zinc Oxide Nanobelts

Among nanostructured semiconducting oxides, ZnO nanostructures have been widely explored because of their interesting physical and electronic properties, such as wide bandgap (~3.37 eV at room temperature), strong piezoelectric, pyroelectric properties, etc. On the other hand, in the chemical sensing direction, chemisensors built on ZnO nanostructures have also attracted intensive attention due to good sensitivity to important industrial gases, such as H_2, NH_3, CO, and H_2S. It is desirable to generate high-quality and single-crystalline ZnO nanostructures for the above-mentioned applications based on ZnO nanomaterials. Thus, numerous approaches, for example, electrochemical, vapor phase growth, and liquid phase growth methods, have been developed toward this direction in the past few years [68]–[70].

ZnO nanobelts grown on alumina plate were first reported by Pan *et al.* [25] using a thermal evaporation method. Zinc oxide powder without the presence of catalysts was placed in an alumina tube that was inserted in a tube furnace, and the growth was carried out under low pressure (~300 torr) at 1400 °C. Without the aid of catalysts, the growth of ZnO nanobelts was governed by the VS process. Fig. 2(a) is an SEM image of as-grown ZnO nanobelts, revealing wire-like morphology with the lengths of several tens to several hundred micrometers. Both energy dispersive X-ray spectroscopy (EDS) and XRD results showed that the as-grown sample was wurtzite crystal structured ZnO nanobelts with the lattice constants of $a = 3.249$ Å and $c = 5.206$ Å, consistent with bulk ZnO. TEM images in Fig. 2(b)–(d) exhibit their belt-like shapes with a uniform width of 50–300 nm along the entire length, and the surface of these nanobelts are clean, suggesting the absence of any sheathed amorphous phase.

B. Indium Oxide Nanowires

Li *et al.* [29] reported the synthesis of In_2O_3 nanowires by laser ablation method. Fig. 3(a) shows a typical SEM image

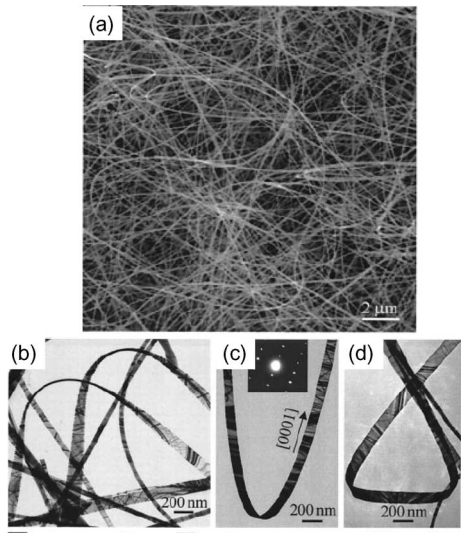

Fig. 2. (a) SEM image of the as-synthesized ZnO nanobelts obtained from thermal evaporation of ZnO powder at high temperature. (b)–(d) TEM images of several straight and twisted ZnO nanobelts, displaying the shape characteristics of the belts (adapted from [25] with permission).

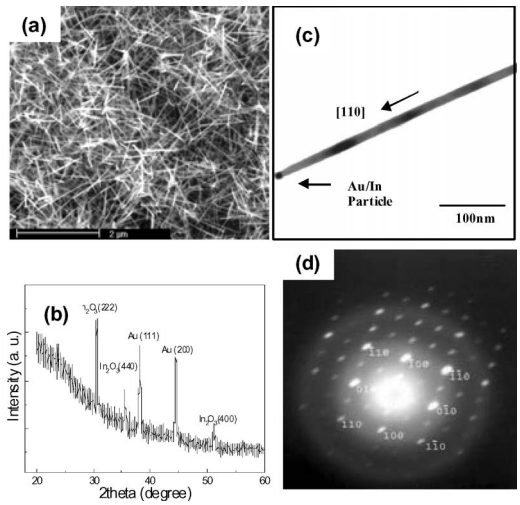

Fig. 3. (a) SEM image of In_2O_3 nanowires grown by laser ablation on an Si/SiO_2 substrate coated with 20 Å Au film. (b) XRD pattern of In_2O_3 nanowires on an Si/SiO_2 substrate. Indexes of the peaks are marked above the peaks. Au peaks come from the catalyst. (c) TEM image of an In_2O_3 nanowire with a catalyst particle at the very tip. The scale bar is 100 nm. The lattice spacing is consistent with the lattice constant (10.1 Å) for bulk In_2O_3. (d) Electron diffraction pattern of the In_2O_3 nanowire indicating the single-crystalline nature (reprint permission from [29]).

of the In_2O_3 nanowires grown on an Si/SiO_2 substrate with 5 nm evaporated Au film. Straight nanowires were found to cover the whole substrate. As-grown nanowires had diameters in the range of 30–50 nm and lengths exceeding 3 μm, indicating an aspect ratio of more than 100:1. XRD was utilized to examine their crystal structure and all samples had similar XRD patterns, as shown in Fig. 3(b). The four major diffraction peaks in the pattern can be indexed to the (2 2 2), (4 0 0), (4 4 0), and (6 2 2) crystal planes of cubic structured In_2O_3 crystal with a cell constant of $a = 1.01$ nm [71]. Besides, two gold peaks from the Au catalysts were also identified. No diffraction peaks from InAs could be found, indicating the high purity of the synthesized In_2O_3 nanowires. EDS was also performed to analyze the composition of the nanowires, and no peaks corresponding to As were detected down to the limit of the equipment.

To make nanowire-based FETs, nanowires with diameters below 30 nm are usually required because of the finite depth a gate electric field can penetrate. This was achieved by using monodispersed gold clusters instead of evaporated gold films. Fig. 3(c) is a TEM image of a single In_2O_3 nanowire synthesized from a 10 nm Au cluster. The Au/In alloy particle, with a diameter around 10 nm, can be clearly seen at the tip of the nanowire. The In_2O_3 appeared rather homogeneous without any domain boundaries, indicating the single-crystalline nature of our material, as expected from the VLS growth mechanism. The nanowire diameter ($\sim$10 nm) is consistent with the diameter of the catalytic particle. The highly crystalline nature of our In_2O_3 nanowires was further confirmed by SAED. Fig. 3(d) shows an SAED pattern, recorded perpendicularly to a nanowire long axis, which indicates the single-crystalline nature of the synthesized In_2O_3 nanowires having a cubic crystal structure with a lattice constant of 1.03 nm, consistent with the XRD results [61]. In addition, unlike Si nanowires usually coated with native oxide, In_2O_3 nanowires are exposed to the ambient. This important difference leads to significant results such as reliable electrical contacts and superior chemical sensing properties for In_2O_3 nanowires.

C. Tin Oxide Nanowires

SnO_2 is a very important n-type semiconductor with a large bandgap ($E_g = 3.6$ eV at 300 K [72]), thus making it ideal for transparent conducting electrodes in organic light-emitting diodes and solar cells [73]. SnO_2 thin films have been extensively studied and used as chemical sensors for environmental and industrial applications [74]. Liu *et al.* [30] suggested that SnO_2 in the nanowire form has enormous potential for nanoelectronics, and also offers superior chemical sensing performance due to the enhanced surface-to-volume ratios.

Fig. 4(a) shows a typical SEM image of SnO_2 nanowires synthesized by the laser ablation method and grown atop the Si/SiO_2 substrates covered with gold clusters [30]. Most of the nanowires have smooth sidewalls and appear rather straight with diameters around 20 nm and lengths in the order of 10 μm, indicating an aspect ratio of $\sim$500:1. Further analysis by XRD is depicted in Fig. 4(b). Six of the diffraction peaks can be indexed to the (1 1 0), (1 0 1), (2 0 0), (2 1 1), (2 2 0), and (3 1 0) crystal planes of the rutile structure of bulk SnO_2 with lattice constants $a = b = 4.750$ Å, and $c = 3.198$ Å [75].

TEM examination determines the nanowire crystal structure and confirms the VLS growth mechanism, as depicted in Fig. 3(c), where an Au/Sn alloy can be found attached to the tip of the nanowire. The nanowire appeared homogeneous and free of domain boundaries under TEM observation even with the sample tilted, indicating the single-crystalline nature of nanowires. This is further confirmed by the sharp SAED pattern (Fig. 4(c), lower inset) recorded perpendicularly to the nanowires long axis. More than 50 nanowires were examined and a histogram of the diameter distribution is shown in the

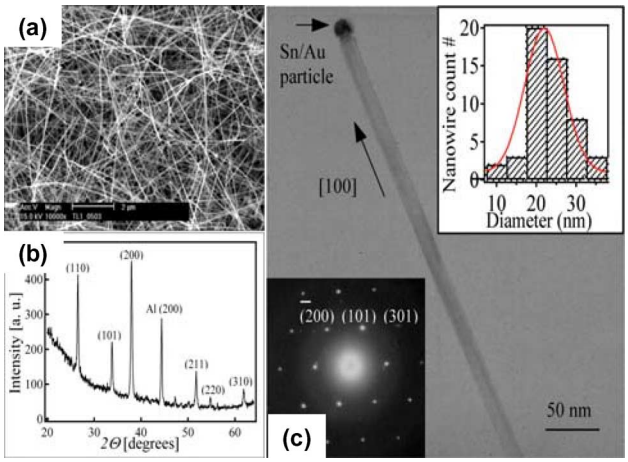

Fig. 4. (a) SEM image of tin oxide nanowires grown on an Si/SiO_2 substrate. (b) XRD pattern of SnO_2 nanowires obtained on Si/SiO_2 substrate. (c) TEM image of an SnO_2 nanowire with a catalyst at the tip. (Lower inset) SAED pattern taken perpendicular to the nanowire long axis. (Upper inset) Histograms of the nanowire diameter distributions. The solid line is a Gaussian fit (reprint permission from [30]).

upper inset of Fig. 4(c). It was found that the majority of the nanowires have diameters between 20 and 25 nm, and the distribution can be well fitted with a Gaussian curve peaked at 22.4 nm. The results convincingly demonstrated the precise control over the diameter of the nanowires, which can be easily achieved by using monodispersed gold clusters, an important advantage of the VLS approach.

III. Electronic Properties of 1-D Metal Oxide Nanostructures

With the success of producing 1-D metal oxide nanostructures, 1-D nanostructure-based FETs can be made readily. In Table II, we summarize the metal-oxide-nanowire-based FETs described in literature and their corresponding electronic transport properties. Among them, transistors made of In_2O_3 nanowires, ZnO nanowires, and SnO_2 nanowires have been widely reported. In comparison with other metal oxide nanomaterials, as one can see, FETs fabricated with these three materials exhibit high electron mobility, high transconductance, and low threshold voltage (not shown here), which are important for applications of nanoelectronics. Besides, there is still a challenge to develop p-type metal oxide nanomaterials with good electronic performance. Doping is a good approach to achieve p-type nanowires (Table II). For instance, Xiang *et al.* reported p-type ZnO nanowires with P as dopant during synthesis with a mobility of 1.7 $cm^2/V{\cdot}s$ and a carrier concentration of 2.2×10^7 cm^{-1}.

Here, FETs built on In_2O_3 nanowires are used as examples to illustrate the electronic properties of 1-D metal oxide nanostructures. The AFM image of Fig. 5(a) inset shows an In_2O_3 nanowire contacted by two metallic electrodes (Ti/Au) patterned atop the Si/SiO_2 substrate. These electrodes are used as the source–drain electrodes while the silicon substrate is used as a back gate. Fig. 5(a) shows the gate-dependent I–V_{ds} curves of the device measured at room temperature. With the gate voltage varying from $+15$ to -10 V, the conductance of the nanowire was gradually suppressed. This behavior is in agreement with the well-known fact that In_2O_3 is an n-type semiconductor due to the O_2 deficiency [76]. Detailed analysis of the transistor data reveals an ON/OFF ratio of 2.08×10^4, a carrier concentration of 2.30 nm^{-1}, and a mobility of 98.1 $cm^2/V{\cdot}s$.

In addition, In_2O_3 is known to be one of the best candidates for transparent electronic applications due to its large bandgap ($\sim$3.6 eV at room temperature). Fig. 5(b) shows the optical photograph of transparent In_2O_3 nanowire transistors with indium-tin-oxide (ITO) electrodes patterned atop a high-k dielectric layer (50 nm HfO_2) on an ITO/glass substrate, showing very good transparency [62]. I–V_{ds} curves of one device with the gate voltage varied from -5 to 5 V are shown in Fig. 5(c), which displays a high ON-current of $\sim$3.8 μA at 2 V with zero gate voltage. Fig. 5(d) is the linear-scale and log-scale drain current versus gate voltage (I_{ds}–V_g) characteristics for the same In_2O_3 nanowire transistor at $V_{ds} = 100$ mV. Detailed analysis revealed an ON/OFF ratio $\sim 10^5$, a mobility of 168.7 $cm^2/V{\cdot}s$, and a threshold voltage of -1.8 V. The electronic performance of these transparent In_2O_3 nanowire transistors is comparable with or even better than traditional In_2O_3 nanowire transistors, made using low-k dielectric and nontransparent electrodes.

Several approaches have been reported suggesting that the electronic performance of nanowire-based transistors can be improved using some postfabrication treatments such as thermal annealing under vacuum [89] or exposure to UV ozone [90]. After exposure to UV ozone for 2 min, the device performance parameters, including ON/OFF ratio, mobility, and subthreshold slope of one In_2O_3 transistor, were enhanced to 10^6, 514 $cm^2/V{\cdot}s$, and 160 mV/decade, respectively.

IV. Chemical Sensing Behavior of 1-D Metal Oxide Nanostructures

Both thin-film and bulk semiconducting metal oxide materials have been widely used for the detection of a wide range of chemicals such as NO_2, NH_3, H_2, H_2S, CO, ethanol, acetone, human breath, and humidity. The sensing mechanism of metal oxide materials mainly relies on the change of electrical conductivity contributed by interactions between metal oxides and surrounding environment. The conductance of 1-D metal oxide nanomaterials can be expressed as [91]

$$G = n_0 e \mu \frac{\pi (D - 2w)^2}{4l} \tag{1}$$

where n_0 represents carrier concentration, μ represents mobility, l is the length of the nanomaterials, D is the diameter of the nanomaterials, and w is the width of surface charge region that is related to the Debye length of the nanomaterials. The Debye length of sensing materials can be expressed as the following formula obtained in the Schottky approximation [92]:

$$w = L_D \left(\frac{eV_s}{kT} \right)^{1/2} \tag{2}$$

$$L_D = \left(\frac{\varepsilon \varepsilon_0 kT}{e^2 n_0} \right)^{1/2} \tag{3}$$

TABLE II
SUMMARY OF THE ELECTRONIC PROPERTIES OF DIFFERENT METAL-OXIDE-NANOMATERIALS-BASED FETS

Materials	Carrier Concentration	Mobility ($cm^2/V•S$)	Transconductance (μS)	Synthesis Method	Ref
ZnO (n-type)	5×10^{15} cm^{-3}	1175	0.06	Thermal CVD	[78]
ZnO:P (p-type)	2.2×10^{7} cm^{-1}	1.7	0.1	Thermal CVD	[79]
ZnO:Ga (n-type)	3.9×10^{18} cm^{-3}	10.2	N/A	Thermal CVD	[80]
In_2O_3 (n-type)	8.56×10^{7} cm^{-1}	1450	5.87	Laser Ablation	[81]
In_2O_3 (n-type)	1.02×10^{7} cm^{-1}	71	1×10^{-3}	Laser Ablation	[29]
SnO_2 (n-type)	2.98×10^{7} cm^{-1}	172	0.18	Laser Ablation	[82]
SnO_2 (n-type)	1.5×10^{8} cm^{-1}	40	3.1×10^{-3}	Laser Ablation	[30]
SnO_2:Ta (n-type)	N/A	156	2.94	Thermal CVD	[83]
T_iO_2 (n-type)	4.5×10^{17} cm^{-3}	0.2	3×10^{-3}	Thermal CVD	[84]
V_2O_5 (n-type)	N/A	9.6×10^{-3} (192K)	N/A	Solution Synthesis	[85]
Ga_2O_3 (p-type)	5.3×10^{8} cm^{-1}	9.6×10^{-2}	9.88×10^{-8}	Thermal CVD	[86]
α-Fe_2O_3 (n-type)	1.59×10^{8} cm^{-1}	9.6×10^{-3}	8.2×10^{-6}	Thermal CVD	[87]
α-Fe_2O_3 (p-type)	4.9×10^{6} cm^{-1}	3.09×10^{-2}	2.2×10^{-3}	Thermal CVD	[88]

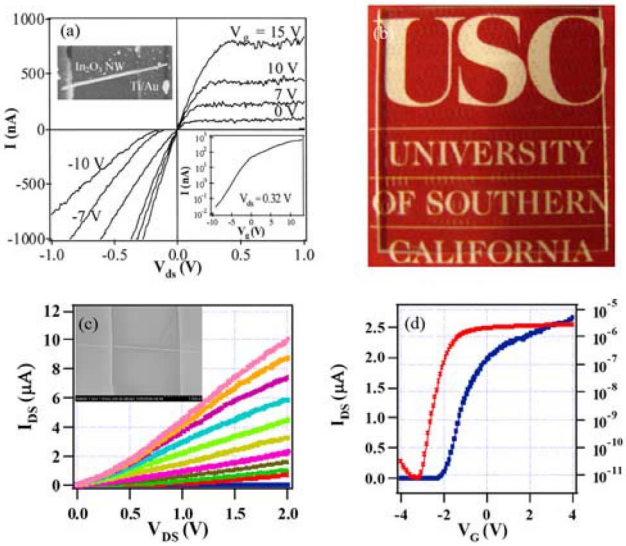

Fig. 5. (a) Gate-dependent I–V curves of a single-In_2O_3-nanowire FET recorded at room temperature. The lower inset shows the current versus gate voltage at $V_{\rm ds} = 0.32$ V. The gate modulated the current by five orders of magnitude. The upper left inset is an AFM image of the In_2O_3 nanowire between two electrodes (reprint permission from [29]). (b) Photograph of transparent In_2O_3 nanowire FETs. (c) Gate-dependent I–V curves recorded with varied gate voltages from −5 to 5 V with step of 1 V. The inset SEM image shows an In_2O_3 nanowire between two ITO electrodes. (d) Linear-scale (blue) and log-scale (red) $I_{\rm ds}$–$V_{\rm g}$ characteristics of an In_2O_3 nanowire transistor at $V_{\rm ds} \sim 100$ mV [77].

where ε_0 is the absolute dielectric constant, ε is the relative dielectric permittivity of the structure, k is the Bolzmann's constant, T is the temperature, and V_S is the adsorbate-induced band bending.

Generally speaking, the response of the chemoresistors in ambient environment can be defined as

$$S = \frac{G_1 - G_0}{G_0} = \frac{4}{D}(w_0 - w_1) = \frac{4}{D}\left(\frac{\varepsilon\varepsilon_0}{en_0}\right)^{1/2}\left(V_{S0}^{1/2} - V_{S1}^{1/2}\right) \quad (4)$$

where G_0 and G_1 are the conductance before and under exposure to chemicals, n_0 and n_1 represent the carrier concentration before and under exposure to chemicals, w_0 and w_1 represent the width of surface charge region before and under exposure of chemicals, V_{S0} is the adsorbate-induced band bending due to oxygen molecule and moisture ($V_{S0} \sim 0.1$ eV [93]) in ambient environment, and V_{S1} is the adsorbate-induced band bending from exposure of chemicals (e.g., NH_3 ~ 0.25 eV [94]).

As one can see in (4), the sensing response can be clearly attributed to three different parts in the right term of the equation, including geometric factor ($4/D$), electronic transport characterizations of nanomaterials ($\varepsilon\varepsilon_0/en_0$), and adsorbate-induced band bending ($V_{S0}^{1/2} - V_{S1}^{1/2}$) due to molecular adsorptions and reactions on metal oxide material surface. The detail of reactions of chemisorbed molecules on nanomaterial surface can be found in [92].

According to (4), there have been a number of approaches developed to improve sensitivity, such as applying an external gate voltage [95], [96], doping metal impurities during material growth [91], modulating operation temperature [97], and changing the geometric structures of nanomaterials [98]. For instance, as one can see in Table III, the detection limit of a ZnO nanowire sensor to NO_2 is tenfold better than the detection limit of a ZnO nanorod sensor because nanowire has a higher surface-to-volume ratio than a nanorod. And also an In_2O_3 porous nanotube film sensor exhibits a 100-fold better sensitivity than a nanowire mat sensor to ammonia at room temperature.

Typically, the detection limits of chemical sensors are also related to the SNR, which has been discussed in carbon-nanotube-based chemical sensors [99]. However, until now, works addressing the noise level of metal-oxide-based chemical sensors have been lacking. This is still a task that needs to be considered in this field.

Table III summarizes some important characterizations of metal oxide nanostructured materials with various sensor types, different geometric structures, and measuring environments. It is not easy to compare the sensing results from different groups due to different material characterizations and electronic transport properties, and a lack of standard procedure for gas testing. For example, instead of humid air (50% RH), some research

TABLE III
GAS SENSORS BASED ON QUASI-1-D METAL OXIDE NANOMATERIALS

Material	Material Type	Sensor Type	Target Gas	Media	Detection Limit	Response Time	12Ref. 1
ZnO	Nanorods	Chemoresistor	NO_2 NO N_2O	Air	10 ppm (125°C)	30 sec	[138]
			Et-OH		1 ppm(350 °C)	N/A	[104]
			H_2S		0.1 ppm (RT) 0.05 ppm (130 °C)		
	Nanowires	FET	NO_2 NH_3	Ar	1 ppm 0.5%	N/A	[95]
	Nanowires	Chemoresistor	Ozone	Humid air	150 ppb (350 °C)	N/A	[105]
	Multi-nanowires		Et-OH	Air	1 ppm (300 °C)	N/A	[106]
	Nanowire Paste		HCHO LPG 90 gasoline CO NH_3		50 ppm 500 ppm 50 ppm (330 °C) 500 ppm 50 ppm	N/A	[102]
Pd-ZnO	Multi-nanorods		H_2	N_2	10 ppm	N/A	[103]
Pt-ZnO	Multi-nanorods		H_2		500 ppm	N/A	[98]
In_2O_3	Single nanowire	FET Chemoresistor	NH_3 NO_2	Air	0.02% 20 ppb	2 min 20 min	[42] [100]
	Single nanowire	Chemoresistor	CO H_2 Et-OH	Air	10 ppm 500 ppm (275 °C) 1 ppm	<1 min	[97]
			CH_4 H_2S HCHO		50 ppm (250 °C)	N/A	[107]
			NO N_2O		0.1 ppm (150 °C)	20 sec	[138]
			Ozone	Humid air	75 ppb (400 °C)	N/A	[106]
	Multi-nanowires		NH_3 NO_2	Air	500 ppm 5 ppb	6 min 16 min	[100]
			Acetone	Humid air	25 ppm (400 °C)	6 min 16 min	[108]
	Porous nanotube film		NH_3	N_2	5 ppm	20 sec	[109]
WO_3	Nanowire	Chemoresistor	NO_2 NO N_2O	Air	0.1 ppm (250 °C)	10 sec	[138]
$WO_{2.72}$	Nanowire		H2S	Humid air	1 ppm (250 °C)	< 100 sec	[101]
TiO_2	Nanowire	Chemoresistor	Et-OH	Air	2% (550 °C)	N/A	[110]
	Nanobelt		O_2	N_2	200 ppb	N/A	[111]
	Nanotube		H_2	N_2	1000 ppm (290 °C)	150 sec	[112]
	Mat-nanofibers	Chemoresistor	NO_2	Air	1ppb (300 °C)	N/A	[113]
SnO_2	Single nanowire	Chemoresistor	CO NH_3	Air	25 ppm (280 °C) 100 ppb (300 °C)	N/A	[114]
			CO NO_2	Humid air	0.1 ppm (400 °C)	N/A	[49]
			Ozone		75 ppb (400 °C)	N/A	[106]
		AC Impedance	CO humidity		100 ppb (300 °C) 15 % (295 °C)	N/A	[115]
	Nanoribbon	Chemoresistor	NO_2	Air	3 ppm (photoinduced)	< 1min	[116]
	Nanobelt		DMMP	Air	78 ppb (500 °C)	N/A	[43]
	Nanotube		NH_3 Et-OH		10 ppm (200 °C) 10 ppm (200 °C)	5 sec	[117]
	Nanorods		Et-OH		10 ppm (300 °C))	N/A	[118]
	Multi-nanowhisker		Et-OH		50 ppm (300 °C)	N/A	[119]
	Nanofiber film		Et-OH		100 ppb (300 °C)	N/A	[120]
SnO_2:In	Multi-nanowire		Et-OH		10 ppm (400 °C)	2 sec	[121]
SnO_2:Sb			Et-OH		10 ppm (300 °C)	N/A	[122]
Au-SnO_2	Nanobelt		CO		50 ppm (400 °C)	~ 1 min	[123]
V_2O_5	Nanobelts	Chemoresistor	Et-OH	Air	5 ppm (400 °C)	30~50 sec	[124]
	Nanofibers		1-butylamine a-propanol Tolune NH_3	N_2	30 ppb 1000 ppm 1000 ppm 10 ppm	N/A	[125]
CuO	Nanoribbons	Chemoresistor	HCHO	Air	5 ppm	N/A	[126]

groups carried out the sensing experiments in vacuum, nitrogen, or dry air environments without consideration of moisture adhesion on nanomaterials surface, which is different in real environments for practical applications and also influenced the sensing results. Besides, different groups have different definitions of response time. For instance, Zhang *et al.* reported a very long response time of 1000 s since they defined the response time corresponding to a decrease of the resistance down to 80% of the original value [100], while another group adopted 90% difference from original value as response time [101], [102]. The difference in definitions may generate confusion about the performance of different chemical sensors. It would be better if there was a standard testing procedure for chemical sensors in the community.

As shown in Table III, in comparison of sensors made of Pt–ZnO thin films (∼20 nm), Pt–ZnO nanorods (diameter: 50–150 nm) based sensors achieved a threefold increase of sensitivity due to higher surface-to-volume ratio of nanorods [98]. However, the detection limits of these metal oxide nanostructured sensors to some chemicals are still far behind the detection limits required by the U.S. Department of Health and Human Services. For example, the Agency for Toxic Substances and Disease Registry (ATSDR) minimal risk levels (MRLs) of formaldehyde (HCHO) is 0.04 ppm, which is far beyond the detection limits reported from CuO nanoribbon sensors (5 ppm [127]), In_2O_3 nanowire sensors (50 ppm [108]), and ZnO nanowire paste sensors (∼50 ppm [101]). Much work still needs to be done to improve the sensing detection limits.

In the following sections, the chemical sensing behavior of several extensively studied 1-D metal oxide nanostructured materials will be discussed.

A. 1-D ZnO Nanostructure Sensors

Among metal-oxide-based chemical sensors, ZnO has been intensively studied for the detection of a host of inflammable and toxic chemicals. Chemical sensors based on 1-D ZnO nanostructures are able to detect both reducing and oxidizing gases and follow the same sensing mechanism as In_2O_3-nanostructure-based sensors.

Fan and Lu [95] studied oxygen and NO_2 adsorption on the ZnO nanowire surface by using individual ZnO nanowire FETs. A considerable variation of conductance was observed when the device was exposed to oxygen or NO_2. In addition, an electrical potential to the back gate electrode was applied, which could help to adjust the sensitivity range of the device or initialize the device completely before exposure to chemicals. For instance, a ZnO chemical sensor was fully refreshed by applying a high negative gate bias of 60 V, as shown in Fig. 6. Besides, the authors also reported that the sensitivity was increased with a decreasing gate voltage while a gate voltage was applied above the device threshold voltage.

Because of the demand for renewable energy resources, instead of NO_2, detection of hydrogen has already attracted a great attention. Pearton and coworkers studied Pt-, Pd-coated, and pristine ZnO nanorods as hydrogen sensors [98], [103]. With the aid of catalytic Pt or Pd coated on the nanowire surface, the sensitivity can be improved by a factor of 3 compared with traditional ZnO thin-film sensors operated at room temperature [98]. This can be attributed to the enhancement of dissociation efficiency of molecular hydrogen to reactive atomic form. These sensors showed reducing response while hydrogen was introduced into the sensing chamber. The reducing response may be attributed to the fact that hydrogen introduces a shallow donor state in ZnO nanorods and contributes to the conductance increase of ZnO-nanorod-based devices.

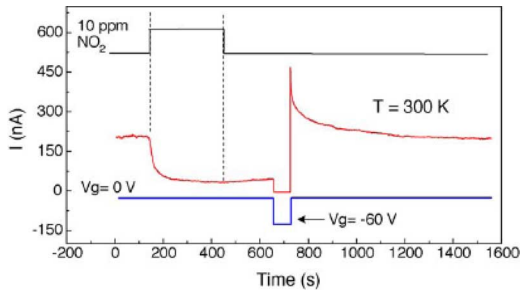

Fig. 6. Response of a ZnO nanowire FET exposed to 10 ppm NO_2 gas. After applying a gate voltage pulse with 60-s duration, the conductance is turned off followed by a current surge. In about 4 min, the conductance recovers to the initial level. The sensing experiments were carried out in dry air (reprint permission from [95]).

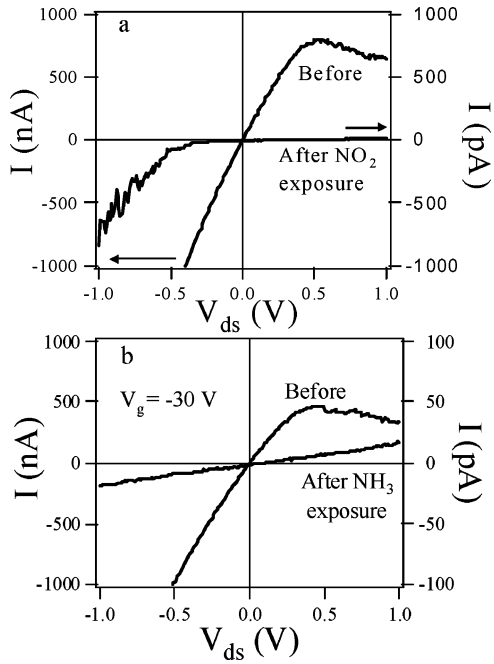

Fig. 7. Single-In_2O_3-nanowire chemical sensor. (a) I–V curves measured before and after exposure to 100 ppm NO_2. (b) I–V curves measured before and after exposure to 1% NH_3 with $V_g = -30$ V. The arrows inside indicate different scales used for the curves. The authors carried out the experiment at room temperature using dry air as carrier gas and purge gas. The flow rate of the chemical here is about 200 sccm (reprint permission from [42]).

B. In_2O_3 Nanowire Sensors

Li *et al.* [42] have demonstrated a chemical sensor built upon an In_2O_3 FET in 2003. Fig. 7(a) shows the I–V curves recorded before and after exposing the nanowire device to 100 ppm NO_2

in Ar for 5 min with 0 V applied to the gate electrode. Different scales (left axis for the curve before the exposure and right axis for the curve after the exposure) were used to elucidate the change in the current magnitude.

The I–V curve recorded before the exposure is typical for In_2O_3 nanowire FETs with a well-defined linear regime and a saturation regime under the positive bias. The asymmetry in the I–V curve is due to the local gating effect, similar to the pinch-off effect of conventional silicon-based FETs [127]. After the exposure, the device showed a reduction in conductance around six orders of magnitude for $V_{ds} = 0.3$ V, as manifested by the data shown in Fig. 7(a). After each exposure, the device was easily recovered to its initial status within a short time by pumping down the system to vacuum followed by UV illumination to desorb the attached NO_2 molecules.

The underlying physics is that UV exposure generates electron and hole pairs in the nanowire, and the adsorbed NO_2 molecules undergo the transition from NO_2^- to NO_2 by taking one hole and leave the nanowire surface. This recovery mechanism works for all sorts of adsorbed species such as NO_2, NH_3, O_2, and moisture. Fig. 7(b) depicts two curves recorded before and after exposure to NH_3 gases with the gate bias maintained at -30 V. A reduction in conductance of five orders of magnitude for $V_{ds} = -0.3$ V was obtained. The enhanced sensitivity is primarily attributed to the enhanced surface-to-volume ratio due to the small diameter (10 nm) of In_2O_3 nanowires. An additional reason is related to the nature of the In_2O_3 nanowire surface that can readily react with ambient species, as compared to the inert sidewall of carbon nanotubes [128].

In order to explore the detection limit and improve the device yield, Zhang *et al.* [100] reported an ultrasensitive NO_2 sensor based on In_2O_3 nanowire networks. Fig. 8(a) plots the changes in nanowire conductance normalized by the initial conductance (G_0) at gate bias $V_g = 0$ V as a function of time. Six cycles were successively recorded, corresponding to six different NO_2/air concentrations ranging from 5 to 200 ppb, respectively. The multiwire sensor showed an even lower detection limit of 5 ppb, compared to the 20 ppb limit of single-nanowire sensors [99].

Detailed examination showed a normalized conductance change ~20% to 5 ppb NO_2 in air, with a response time of ~1000 s, defined as the time corresponding to a decrease of the resistance down to 80% of the original value. This room temperature detection limit to NO_2 is the lowest level achieved so far with all metal oxide film or nanowire sensors. The authors attributed the improved sensitivity to the formation of nanowire/nanowire junctions between the metal electrodes, a feature available in the multiple nanowire devices [Fig. 8(b)] but missing in the single-nanowire devices. Such junctions, when exposed to NO_2, should form a depleted layer around the intersection and thus block the electron flow in a way more prominent than the surface depletion of single nanowires with metal contacts.

To reach practical applications of metal oxide nanowire sensors, operating the nanosensors at elevated temperature with minimal inconvenience and low power consumption is very important. Ryu *et al.* proposed a facile integration of nanowire

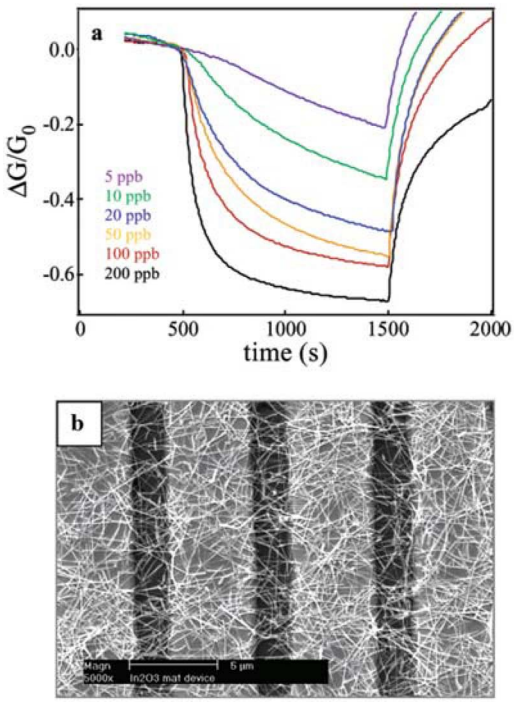

Fig. 8. (a) Six sensing cycles of a multi-In_2O_3 nanowire device, corresponding to NO_2 concentrations of 5, 10, 20, 50, 100, and 200 ppb. (b) SEM image of the as-fabricated multiwire devices, where bulk quantity (10^2–10^3) of In_2O_3 nanowires is contacted by four electrodes. The authors carried out the experiment at room temperature and used dry air for both carrier gas and purge gas. The flow rate of the chemicals is about 200 sccm (reprint permission from [100]).

chemical sensors with micromachined hot plates built on SiN membranes. The details can be found in literature [97]. Fig. 9(a) is an SEM image of the active area of one chemical sensor chip, where the dashed box represents the SiN membrane and one nanowire is bridged by two electrodes that can be used as a chemical sensor, as shown in Fig. 9(b).

The performance of these microelectromechanical systems (MEMS) hot plates can be evaluated by measuring the hot plate temperature as a function of the power consumption. As one can see in Fig. 9(c), only 60 mW of power is enough to raise the heater temperature up to 300 °C within 1 min, which is much lower than the chemical sensors based on the KAMINA technique [9], [10]. With the aid of micromachined hot plates, the detection limit of ethanol can be down to 1 ppm while the operating temperature is at 275 °C [Fig. 9(d)].

C. 1-D SnO_2 Nanostructure Sensors

SnO_2 nanowires and nanobelts have been widely reported as chemical sensors in a number of reports [129]–[131]. The first SnO_2 nanobelt chemical sensor was made on an alumina substrate by dispersing SnO_2 nanobelts atop prefabricated platinum interdigitated electrodes on a substrate. The sensor was employed to detect CO and NO_2 for environmental polluting species and ethanol for breath analysis. In 2005, Yu *et al.* [43] reported a single-SnO_2-nanobelt sensor integrated with

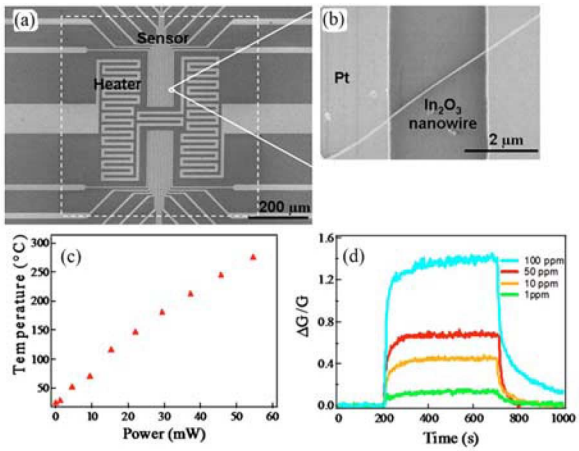

Fig. 9. (a) SEM image of the chemical sensor chip integrated on single-In_2O_3 nanowire and micromachined hot plates, where the dashed box indicates the SiN membrane. (b) SEM image of a sensing device with an In_2O_3 nanowire bridging two electrodes. (c) Hot plate temperature as a function of the power consumption of the Pt heater. (d) Sensing response of an In_2O_3 nanowire sensor operated at 275 °C to four different ethanol concentrations (1, 10, 50, and 100 ppm). The normalized conductance change ($\Delta G/G$) of an In_2O_3 nanowire is plotted as a function of time (d). The authors carried out the experiment at room temperature and used dry air for both carrier gas and purge gas (adapted from [97] with permission).

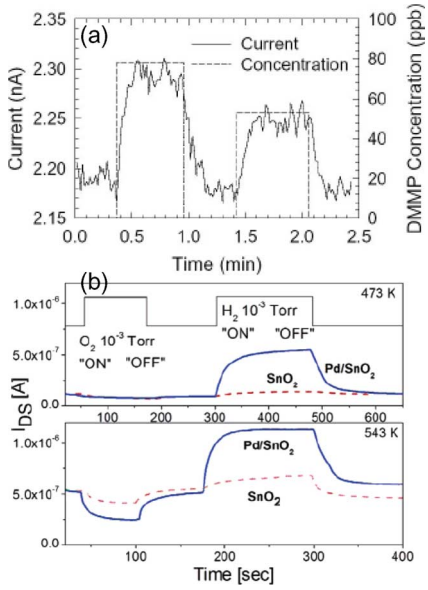

Fig. 10. (a) Response of the SnO_2 nanobelt sensor to 78 and 53 ppb DMMP balanced with air at 500 °C. The applied voltage to nanobelt was 1.5 V (reprint permission from [43]). (b) Response of a pristine SnO_2 and Pd–SnO_2 to sequential oxygen and hydrogen pulses at 473 (top) and 543 K (bottom). The sensing experiments were carried out in low-pressure environment with oxygen as back ground gases. The detail can be found in [44] (reprint permission from [44]).

microheaters to sense dimethyl methylphosphonate (DMMP), a nerve agent simulant. The conductance of the SnO_2 nanobelt sensor was reduced by 5% when the sensor was exposed to 78 ppb of DMMP [Fig. 10(a)]. Recently, Wan *et al.* [122] proposed a high-performance ethanol senor based on branched SnO_2/Sb-doped SnO_2 nanowire films. The metallic backbones of Sb-doped SnO_2 dramatically reduced the resistance by a factor of 10^3 and the branched structure offered more pathways for electrical conduction in comparison of pure SnO_2 nanowire films, thus significantly reducing the detectable limit of ethanol to sub-ppm at 300 °C.

Instead of using pristine SnO_2 nanomaterials as chemical sensors, Kolmakov *et al.* demonstrated an enhanced 1-D SnO_2-nanostructure-based sensor with Pd nanoparticles decorated on the surface of nanowires and nanobelts [44]. It is known that Pd can work as catalysts for oxygen dissociation. The catalytic effect of a Pd nanoparticle and sensing capability of functionalized SnO_2 were investigated in detail. Fig. 10(b) shows different sensing responses of Pd–SnO_2 and pristine SnO_2 nanostructures to oxygen and hydrogen, respectively. As one can see, Pd functionalization leads to significant sensing response and also shortens the recovery time. The improvements of sensitivity can be explained by the "spillover effect" and the "back-spillover effect," which are well established in catalysis literature [44]. Through these two processes, the numbers of oxygen ions adsorbed on SnO_2 surface were increased, and thus resulted in shorter response time. In addition to Pd nanoparticle decoration, Ag [132], Ni [91], and Au [123] nanoparticles have also been reported for SnO_2 nanostructure decoration, leading to improved sensitivity of ethylene [130] and CO [122] down to several tens ppm.

D. Other 1-D Metal Oxide Nanostructure Sensors

In addition to the above-discussed nanomaterials, other 1-D metal oxide nanostructures, such as titanium oxide (TiO_2) [110], [113], [133], vanadium oxide (V_2O_5) [124], [125], copper oxide (CuO) [134], [135], and tungsten oxide (WO_3) [136]–[138], have also been investigated and used as chemical sensors.

Several studies on TiO_2 nanowires and nanofibers in the detection of ethanol, hydrogen, and NO_2 have been reported. Tuller *et al.* reported a novel electrospun method to fabricate TiO_2 nanofiber mat sensors [113], which exhibited a sensitivity to NO_2 down to ~1 ppb at 300 °C. The device resistance was found to increase by 833% after the exposure to 500 ppb NO_2. The authors stated that the sensing mechanism of TiO_2 nanofibers is similar to the sensing mechanism of reported n-type semiconducting metal oxides. These electrospun-fabricated TiO_2 nanofiber sensors were also exposed to H_2, CH_4, and DMMP, and the sensing limits of these chemicals were several ppm.

In the case of V_2O_5 nanostructures, Raible *et al.* reported V_2O_5-nanofiber-based sensors that showed a high sensitivity of 30 ppb 1-butylamine at room temperature, and the authors suggested that V_2O_5 nanofibers have a strong affinity to amine species [125]. In addition, Liu *et al.* synthesized V_2O_5 nanobelts using a hydrothermal method, and the V_2O_5 nanobelt chemical sensors showed a good selectivity among ethanol vapor, H_2, and CO [125]. Since V_2O_5 nanostructures showed a good sensitivity and selectivity to amine and ethanol, these nanostructures might be utilized as components in an electronic nose system or for diagnosis of diseases such as uremia and cancers.

Recently, the sensing behavior of CuO nanoribbons produced using a hydrothermal process was also investigated [89]. CuO nanoribbons exhibited a high sensitivity (∼5 ppm) to HCHO, which is a cancer marker for diagnosis of early-stage breast and bladder cancer [126] at room temperature. Besides, the responses with different CuO nanostructures were comparatively studied and CuO-nanoribbon-based sensors showed eight orders of magnitude higher sensitivity than CuO-nanoplate-based sensors [134]. There was almost no significant response to HCHO in commercial bulk CuO-powder-based sensors. The authors believed that this specialty was because of the high surface-to-volume ratio of the intrinsic morphology of CuO nanoribbons.

V. Electronic Noses

A. Concept of Electronic Noses

As illustrated in the section IV, metal oxide nanostructured chemical sensors have shown good sensitivity toward a broad range of chemicals. However, a critical issue in the development of chemical sensor systems for practical applications is the "selectivity." One promising way to achieve selectivity among different chemicals is to build "electronic noses." The idea of electronic noses was inspired by the mechanisms of human olfaction. In general, basic elements of an electronic nose system include an "odor" sensor array, a data preprocessor, and a pattern recognition (PARC) engine [139]. Among them, a sensor array that mimics the olfactory receptor cells situated in the roof of the nasal cavity of human beings is like signal receptors.

The concept of "chemical sensor array" for odor reorganization was demonstrated by Persaud and Dodd [140]. After that, considerable effort has been directed to develop different types of sensor arrays such as chemoresistors, acoustic/SAW sensors, optical sensors, and potentiometric transducers. On the other hand, sensor arrays made by different active materials were also studied. For example, Yu *et al.* [141] and McApline *et al.* [142] have reported using functionalized carbon nanotubes [141] and Si nanowires [142] as active materials for chemical sensor arrays of electronic nose systems.

Sensor arrays made of thin-film metal oxides have been widely discussed [143]–[146], but only limited work on semiconducting-oxide-based sensor arrays has been performed. The following sections review two different sensor arrays that have good "discrimination factors" and successfully recognized the target chemical among different chemicals.

B. Hybrid Nanowire/Carbon Nanotube Sensor Array

To enhance the "discrimination power" of important chemicals, Chen *et al.* [147] studied a new template built with four different semiconducting nanostructured materials, including In_2O_3 nanowires, SnO_2 nanowires, ZnO nanowires, and single-walled carbon nanotubes (SWNT). The integration of n-type semiconducting metal oxide nanowire and p-type semiconducting SWNT provides an important discrimination factor. In addition, the integrated micromachined hot plate enables individual and accurate temperature control for each sensor, thus providing the second discrimination factor. A chemical sensor array, composed of four different sensor chips, each with individual In_2O_3 nanowire, SnO_2 nanowire, ZnO nanowire, and an SWNT mat, was examined using field-emission SEM (FESEM) and optical microscopy (corresponding images are depicted in Fig. 11).

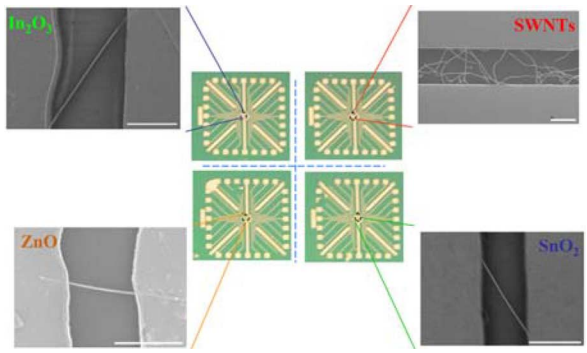

Fig. 11. Hybrid chemical sensor array chip composed of four individual chemical sensors, including individual In_2O_3 nanowire, SnO_2 nanowire, ZnO nanowire, and SWNT chemical sensor chips. The source–drain electrode distance is about 3 μm [147].

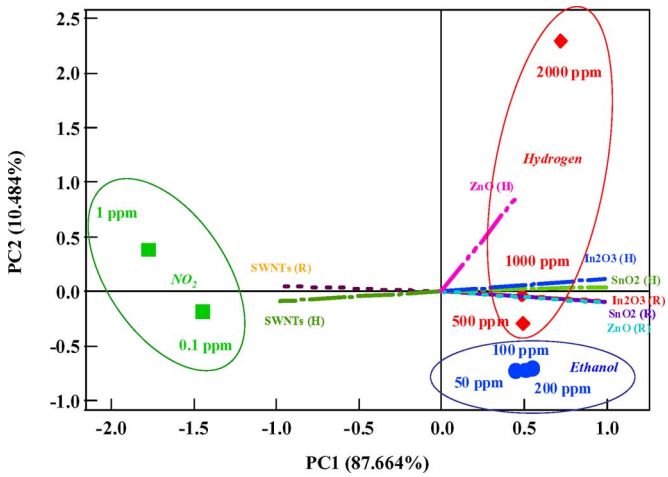

Fig. 12. PCA scores and loading plots of the chemical sensor array composed of four different nanostructure materials [147].

This sensor array was exposed to important industrial gases such as hydrogen, ethanol, and nitrogen dioxide at different concentrations and sensing temperatures, and a good selectivity was obtained to build up an interesting "smell-print" library of these gases. Principal component analysis (PCA) of the sensing results showed great discrimination of those three tested chemicals, and in-depth analysis revealed clear improvement of selectivity, as shown in Fig. 12. This nanoelectronic nose approach has great potential to detect and discriminate a wide variety of gases, including explosives and nerve agents. We note that further improvement to the selectivity can be achieved by incorporating more diverse nanosensors into the electronic nose. For instance, using nanosensors decorated with Pd nanoparticles may help the discrimination between hydrogen and other chemicals.

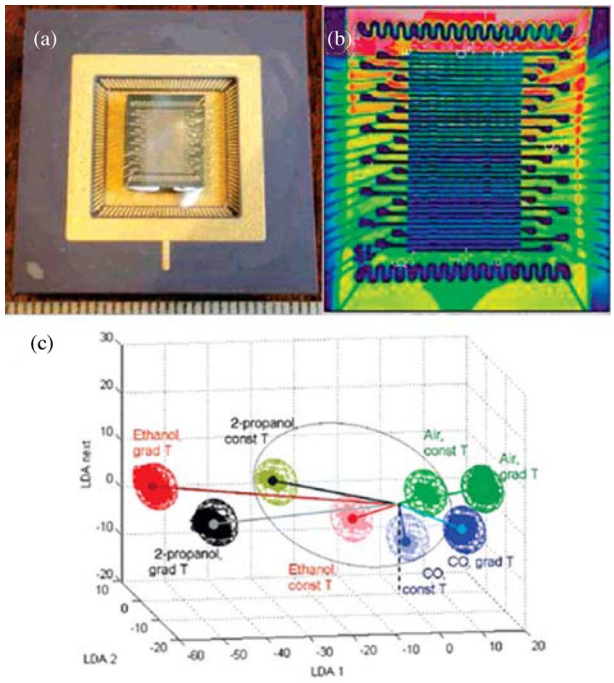

Fig. 13. (a) KAMINA chip with SnO_2 nanowire sensing elements. (b) IR image of the chip under application of the temperature gradient, 520 (green area) to 600 K (red area) along the electrode array. (c) LDA analysis of the conductivity patterns obtained with SnO_2-nanowire-based gradient sensor at exposure to chemicals (2–10 ppm concentration range). The KAMINA chip operates at 580 K (constant T area inside the ellipse with dimmed colors) and at temperature gradient from 520 to 600 K (gradient T areas with bright colors) (adapted from [152] with permission).

C. KAMINA Technology

The key feature of the KAMINA technology [148] is the "temperature gradient technique" applied to a single metal oxide layer that is usually deposited onto an array of Pt strips. Metal oxide layers between two Pt electrodes can serve as an individual sensor element. This technology has been widely applied to both semiconducting oxide thin-film and nanostructure-based sensors [149]–[151].

With the help of the patented KAMINA technology, Sysoev *et al.* [152] reported a platform based on SnO_2 nanowire networks for nanoelectronic–nose systems. The sensor successfully recognized several violate organic compounds (VOCs) such as ethanol, CO, and 2-propanol at elevated temperatures from 520 to 600 K. Fig. 13(a) shows the KAMINA platform with SnO_2 nanowire networks as the sensing elements. SnO_2 nanowires were mechanically transferred onto a KAMINA's $SiO_2/Si/SiO_2$ substrate that was patterned with Pt electrodes. The chip can be heated by applying an external voltage to the rear-side meander-shaped Pt heating filaments. The temperature gradient on a KAMINA chip is clearly observed through an IR detector, as shown in Fig. 13(b). In this paper, the "discrimination factors" were achieved by the variation of the density and also the morphological inhomogeneities of nanowire mats in temperature gradient across the nanowire layer on the sensor chip.

Linear discrimination analysis (LDA) was applied to examine the discrimination power quantitatively and the result is shown in Fig. 13(c). As one can see, the isothermal conductivity patterns are good enough to obtain well-separated signal patterns for various VOCs. With the application of a temperature gradient along the sensor chip, the discrimination power is significantly enhanced, which is attributed to the surface chemistry and the charge transport of SnO_2 nanowire networks [151].

VI. Summary

This review is a report of the current accomplishments on the investigation of 1-D metal oxide nanostructures, ranging from material synthesis and chemical sensing behavior, to the realization of electronic noses. 1-D metal oxide nanostructures of In_2O_3, SnO_2, ZnO, TiO_2, and CuO, have been synthesized using various means and further demonstrated to exhibit very good sensitivity in the detection of industrial gases, chemical wafare agents, and human breath (e.g., NH_3, $HCHO$, H_2S, and ethanol). In addition, several electronic nose systems based on metal oxide nanowires have been developed to address the challenging issues of choice of sensing materials (In_2O_3, SnO_2, ZnO, and carbon nanotubes) and of using the nanowire density variation and temperature gradient. Further improvement of the overall nanowire sensor performance, such as sensitivity and selectivity, will likely generate significant practical impact on environment monitoring, defense applications, and even medical diagnosis.

References

[1] K. Sugiyasu and T. M. Swager, "Conducting-polymer-based chemical sensors: Transduction mechanisms," *Bull. Chem. Soc. Jpn.*, vol. 80, pp. 2074–2083, 2007.
[2] U. Lange, N. V. Roznyatovskaya, and V. M. Mirsky, "Conducting polymers in chemical sensors and arrays," *Anal. Chim. Acta*, vol. 614, pp. 1–26, 2008.
[3] A. Damico and E. Verona, "SAW sensors," *Sens. Actuators*, vol. 17, pp. 55–66, 1989.
[4] M. Penza, F. Antolini, and M. Vittori-Antisari, "Carbon nanotubes-based surface acoustic waves oscillating sensor for vapour detection," *Thin Solid Films*, vol. 472, pp. 246–252, 2005.
[5] E. Comini, "Metal oxide nano-crystals for gas sensing," *Anal. Chim. Acta*, vol. 568, pp. 26–40, 2006.
[6] S. Joo and R. B. Brown, "Chemical sensors with integrated electronics," *Chem. Rev.*, vol. 108, pp. 638–651, 2008.
[7] L. A. Pinnaduwage, A. C. Gehl, S. L. Allman, A. Johansson, and A. Boisen, "Miniature sensor suitable for electronic nose applications," *Rev. Sci. Instrum.*, vol. 78, pp. 055101-1–055101-4, 2007.
[8] P. T. Moseley, J. O. W. Norris, and D. E. Williams, *Techniques and Mechanisms of Gas Sensing*. Bristol, U.K.: Adam Hilger, 1991.
[9] C. Arnold, D. Haeringer, I. Kiselev, and J. Goschnic, "Sub-surface probe module equipped with the Karlsruhe Micronose KAMINA using a hierarchical LDA for the recognition of volatile soil pollutants," *Sens. Actuators B*, vol. 116, pp. 90–94, 2006.
[10] J. Goschnick, D. Haeringer, and I. Kiselev, "Multicomponent quantification with a novel method applied to gradient gas sensor microarray signal patterns," *Sens. Actuators B*, vol. 127, pp. 237–241, 2007.
[11] R. C. Young, W. J. Buttner, B. R. Linnell, and R. Ramesham, "Electronic nose for space program applications," *Sens. Actuators B*, vol. 93, pp. 7–16, 2003.
[12] A. Morales and C. M. Lieber, "A laser ablation method for the synthesis of crystalline semiconductor nanowires," *Science*, vol. 279, pp. 208–211, 1998.
[13] M. Huang, A. Choudrey, and P. Yang, "Ag nanowire formation within mesoporous silica," *Chem. Commun.*, vol. 12, pp. 1063–1064, 2000.

[14] B. H. Hong, S. C. Bae, C. W. Lee, S. Jeong, and K. S. Kim, "Ultrathin single-crystalline silver nanowire arrays formed in an ambient solution phase," *Science*, vol. 294, pp. 348–351, 2001.

[15] Y. J. Hsu and S. Y. Lu, "Vapor–solid growth of Sn nanowires: Growth mechanism and superconductivity," *J. Phys. Chem. B*, vol. 109, pp. 4398–4403, 2005.

[16] J. G. Wang, M. L. Tian, N. Kumar, and T. E. Mallouk, "Controllable template synthesis of superconducting Zn nanowires with different microstructures by electrochemical deposition," *Nano Lett.*, vol. 5, pp. 1247–1253, 2005.

[17] S. Han, W. Jin, T. Tang, C. Li, D. Zhang, X. Liu, J. Han, and C. Zhou, "Controlled growth of gallium nitride single crystal nanowires using a chemical vapor deposition method," *J. Mater. Res.*, vol. 18, pp. 245–249, 2003.

[18] T. Tang, S. Han, W. Jin, X. Liu, C. Li, D. Zhang, C. Zhou, B. Chen, J. Han, and M. Meyyappan, "Synthesis and characterization of single-crystal indium nitride nanowires," *J. Mater. Res.*, vol. 19, pp. 423–426, 2004.

[19] K. A. Dick, K. Deppert, L. S. Karlsson, W. Seifert, L. R. Wallenberg, and L. Samuelson, "Position-controlled interconnected InAs nanowire networks," *Nano Lett.*, vol. 6, pp. 2842–2847, 2006.

[20] P. Mohan, J. Motohisa, and T. Fukui, "Fabrication of InP/InAs/InP core-multishell hetrostructure nanowires by selective area metalorganic vapor phase epitaxy," *Appl. Phys. Lett.*, vol. 88, pp. 133105–133107, 2006.

[21] J. Zhu, H. Peng, C. K. Chan, K. Jarausch, X. F. Zhang, and Y. Cui, "Hyperbranched lead selenide nanowire networks," *Nano Lett.*, vol. 7, pp. 1095–1099, 2007.

[22] X. F. Qiu, Y. B. Lou, A. C. S. Samia, A. Devadoss, J. D. Burgess, S. Dayal, and C. Burda, "PbTe nanorods by sonoelectrochemistry," *Angew. Chem. Int. Ed.*, vol. 44, pp. 5855–5857, 2005.

[23] H. J. Chang, E. J. In, K. J. Kong, J. O. Lee, Y. M. Choi, and B. H. Ryu, "First-principles studies of SnS_2 nanotubes: A potential semiconductor nanowire," *J. Phys. Chem. B*, vol. 109, pp. 30–32, 2005.

[24] M. J. Bierman, Y. K. A. Lau, and S. Jin, "Hyperbranched PbS and PbSe nanowires and the effect of hydrogen gas on their synthesis," *Nano Lett.*, vol. 7, pp. 2907–2912, 2007.

[25] Z. W. Pan, Z. R. Dai, and Z. L. Wang, "Nanobelts of semiconducting oxides," *Science*, vol. 291, pp. 1947–1949, 2001.

[26] S. Han, C. Li, Z. Liu, B. Lei, D. Zhang, W. Jin, X. Liu, T. Tang, and C. Zhou, "Transition metal oxide core-shell nanowires: Generic synthesis and transport studies," *Nano Lett.*, vol. 4, pp. 1241–1245, 2004.

[27] L. Greene, M. Law, D. H. Tan, J. Goldberger, and P. Yang, "General route to vertical ZnO nanowire arrays using textured ZnO seeds," *Nano Lett.*, vol. 5, pp. 1231–1236, 2005.

[28] P. C. Chang, H. Y. Chen, J. S. Ye, F. S. Sheu, and J. G. Lu, "Vertically aligned antimony nanowires as solid-state pH sensors," *Chem. Phys. Chem.*, vol. 8, pp. 57–61, 2007.

[29] C. Li, D. Zhang, S. Han, X. Liu, T. Tang, and C. Zhou, "Diameter-controlled growth of single-crystalline In_2O_3 nanowires and their electronic properties," *Adv. Mater.*, vol. 15, pp. 143–146, 2003.

[30] Z. Liu, D. Zhang, S. Han, C. Li, T. Tang, W. Jin, X. Liu, B. Lei, and C. Zhou, "Laser ablation synthesis and electron transport studies of tin oxide nanowires," *Adv. Mater.*, vol. 20, pp. 1754–1757, 2003.

[31] C. Li, B. Lei, W. Fan, D. Zhang, M. Meyyappan, and C. Zhou, "Molecular memory based on nanowire–molecular wire heterostructures," *J. Nanosci. Nanotechnol.*, vol. 7, pp. 138–150, 2007.

[32] J. Xiang, W. Lu, Y. J. Hu, Y. Wu, H. Yan, and C. M. Lieber, "Ge/Si nanowire heterostructures as high-performance field-effect transistors," *Nature*, vol. 441, pp. 489–493, 2006.

[33] S. Ju, J. Li, J. Liu, P. C. Chen, Y. Ha, F. N. Ishikawa, H. K. Chang, C. Zhou, A. Facchetti, D. B. Janes, and T. J. Marks, "Transparent active matrix organic light-emitting diode displays driven by nanowire transistor circuitry," *Nano Lett.*, vol. 8, pp. 997–1004, 2008.

[34] Y. Huang, X. F. Duan, Y. Cui, L. J. Lauhon, K. H. Kim, and C. M. Lieber, "Logic gates and computation from assembled nanowire building blocks," *Nano Lett.*, vol. 294, pp. 1313–1317, 2001.

[35] N. A. Melosh, A. Boukai, F. Diana, B. Gerardot, A. Badolato, P. M. Petroff, and J. R. Heath, "Ultrahigh-density nanowire lattices and circuits," *Science*, vol. 300, pp. 112–115, 2003.

[36] F. Qian, S. Gradecak, Y. Li, C. Y. Wen, and C. M. Lieber, "Core/multishell nanowire heterostructures as multicolor, high-efficiency light-emitting diodes," *Nano Lett.*, vol. 5, pp. 2287–2291, 2005.

[37] M. H. Huang, S. Mao, H. Feick, H. Q. Yan, Y. Y. Wu, H. Kind, E. Weber, R. Russo, and P. Yang, "Room-temperature ultraviolet nanowire nanolasers," *Science*, vol. 292, pp. 1897–1899, 2001.

[38] A. Jamshidi, P. J. Pauzauskie, P. J. Schuck, A. T. Ohta, P. Chiou, J. Chou, P. Yang, and M. C. Wu, "Dynamic manipulation and separation of individual semiconducting and metallic nanowires using optoelectronic tweezers," *Nature Photon.*, vol. 2, pp. 85–89, 2008.

[39] M. Law, L. E. Greene, J. C. Johnson, R. Saykally, and P. Yang, "Nanowire dye-sensitized solar cells," *Nature Mater.*, vol. 4, pp. 455–459, 2005.

[40] C. Levy-Clement, R. Tena-Zaera, M. A. Ryan, A. Katty, and G. Hodes, "CdSe-sensitized p-CuSCN/nanowire n-ZnO hetrojunctions," *Adv. Mater.*, vol. 17, pp. 1512–1515, 2005.

[41] J. B. Baxter and E. S. Aydil, "Nanowire-based dye-sensitized solar cells," *Appl. Phys. Lett.*, vol. 86, pp. 053114–053116, 2005.

[42] C. Li, D. Zhang, X. Liu, S. Han, T. Tang, J. Han, and C. Zhou, "In_2O_3 nanowires as chemical sensors," *Appl. Phys. Lett.*, vol. 82, pp. 1613–1616, 2003.

[43] C. Yu, Q. Hao, S. Saha, L. Shi, X. Kong, and Z. L. Wang, "Integration of metal oxide nanobelts with microsystems for nerve agent detection," *Appl. Phys. Lett.*, vol. 86, pp. 063101–063103, 2005.

[44] A. Kolmakov, D. O. Klenov, Y. Lilach, S. Stemmer, and M. Moskovits, "Enhanced gas sensing by individual SnO_2 nanowires and nanobelts functionalized with Pd catalyst particles," *Nano Lett.*, vol. 5, pp. 667–673, 2005.

[45] E. Comini, G. Faglia, G. Sberveglier, D. Calestani, L. Zanotti, and M. Zha, "Tin oxide nanobelts electrical and sensing properties," *Sens. Actuators B*, vol. 111–112, pp. 2–6, 2005.

[46] C. S. Rout, K. U. Kulkarni, and C. N. R. Rao, "Room temperature hydrogen and hydrocarbon sensors based on single nanowires of metal oxides," *J. Phys. D: Appl. Phys.*, vol. 40, pp. 2777–2782, 2007.

[47] Q. H. Li, Y. X. Liang, Q. Wan, and T. H. Wang, "Oxygen sensing characteristics of individual ZnO nanowire transistors," *Appl. Phys. Lett.*, vol. 85, pp. 6389–6391, 2004.

[48] M. Law, H. Kind, B. Messer, F. Kim, and P. Yang, "Photochemical sensing of NO_2 with SnO_2 nanoribbon nanosensors at room temperature," *Angew. Chem. Int. Ed.*, vol. 41, pp. 2405–2408, 2002.

[49] J. G. Lu, P. Chang, and Z. Fan, "Quasi-one-dimensional metal oxide materials-synthesis, properties and applications," *Mater. Sci. Eng. R*, vol. 52, pp. 49–91, 2006.

[50] A. Kolmakov, X. H. Chen, and M. Moskovits, "Functionalizing nanowires with catalytic nanoparticles for gas sensing application," *J. Nanosci. Nanotechnol.*, vol. 8, pp. 111–121, 2008.

[51] X. J. Huang and Y. K. Choi, "Chemical sensors based on nanostructured materials," *Sens. Actuators B*, vol. 122, pp. 659–671, 2007.

[52] A. Kolmakov and M. Moskovits, "Chemical sensing and catalysis by one-dimensional metal-oxide nanostructures," *Annu. Rev. Mater. Res.*, vol. 34, pp. 151–180, 2004.

[53] C. A. Berven and V. V. Dobrokhotov, "Towards practicable sensors using one-dimensional nanostructures," *Int. J. Nanotechnol.*, vol. 5, pp. 402–449, 2008.

[54] A. Kolmakov, "Some recent trends in the fabrication, functionalisation and characterization of metal oxide nanowire gas sensors," *Int. J. Nanotechnol.*, vol. 5, pp. 450–474, 2008.

[55] E. Comini, G. Faglia, G. Sberveglieri, Z. W. Pan, and Z. L. Wang, "Stable and highly sensitive gas sensors based on semiconducting oxide nanobelts," *Appl. Phys. Lett.*, vol. 81, pp. 1869–1871, 2002.

[56] C. Lao, Y. Li, C. P. Wong, and Z. L. Wang, "Enhancing the electrical and optoelectronic performance of nanobelt devices by molecular surface functionalization," *Nano Lett.*, vol. 7, pp. 1323–1328, 2007.

[57] P. Qi, O. Vermesh, M. Grecu, A. Javey, Q. Wang, and H. Dai, "Toward large arrays of multiplex functionalized carbon nanotube sensors for highly sensitive and selective molecular detection," *Nano Lett.*, vol. 3, pp. 347–351, 2003.

[58] A. Star, V. Joshi, S. Skarupo, D. Thomas, and J.-C. P. Gabriei, "Gas sensor array based on metal-decorated carbon nanotubes," *J. Phys. Chem. B*, vol. 110, pp. 21014–21020, 2006.

[59] B. Kim, N. Park, P. S. Na, H. So, J. Kim, H. Kim, K. Kong, H. Chang, B. Ryu, Y. Choi, and J. Lee, "The effect of metal cluster coating on carbon nanotubes," *Nanotechnology*, vol. 17, pp. 496–500, 2006.

[60] Y. Sun and H. H. Wang, "High-performance, flexible hydrogne sensors that use carbon nanotubes decorated with palladium nanoparticles," *Adv. Mater.*, vol. 19, pp. 2818–2823, 2007.

[61] J. W. Gardner and P. N. Bartlett, "A brief history of electronic noses," *Sens. Actuators B*, vol. 18/19, pp. 211–220, 1994.

[62] Z. R. Dai, Z. W. Pan, and Z. L. Wang, "Novel nanostructures of functional oxides synthesized by thermal evaporation," *Adv. Funct. Mater.*, vol. 13, pp. 9–24, 2003.

[63] M. Kuno, "An overview of solution-based semiconductor nanowires: Synthesis and optical studies," *Phys. Chem. Chem. Phys.*, vol. 10, pp. 620–639, 2008.

[64] G. Z. Cao and D. W. Liu, "Template-based synthesis of nanorod, nanowire, and nanotube arrays," *Adv. Colloid Interface Sci.*, vol. 136, pp. 45–64, 2008.

[65] C. N. R. Rao, F. L. Deepak, G. Gundiah, and A. Govindaraja, "Inorganic nanowires," *Progr. Solid State Chem.*, vol. 31, pp. 5–147, 2003.

[66] K. Takahashi, S. J. Limmer, Y. Wang, and G. Z. Cao, "Synthesis and electrochemical properties of single-crystal V_2O_5 nanorod arrays by template-based electrodeposition," *J. Phys. Chem. B*, vol. 108, pp. 9795–9800, 2004.

[67] C. Li, D. Zhang, S. Han, X. Liu, T. Tang, B. Lei, Z. Liu, and C. Zhou, "Synthesis, electronic properties and applications of indium oxide nanowires," *Ann. N. Y. Acad. Sci.*, vol. 1006, pp. 104–121, 2003.

[68] P. Chang, Z. Fan, D. Wang, W. Tseng, W. Chiou, J. Hong, and J. G. Lu, "ZnO nanowire synthesized by vapor trapping CVD method," *Chem. Mater.*, vol. 16, pp. 5133–5137, 2004.

[69] M. H. Wong, A. Berenov, X. Qi, M. J. Kappers, Z. H. Barber, B. Illy, Z. Lockman, M. P. Ryan, and J. L. MacManus-Driscoll, "Electrochemical growth of ZnO nano-rods on polycrystalline Zn foil," *Nanotechnology*, vol. 14, pp. 968–973, 2003.

[70] R. Maity, S. Das, M. K. Mitra, and K. K. Chattopadhyay, "Synthesis and characterization of ZnO nano/microfibers thin films by catalyst free solution route," *Phys. E, Low Dimensional Syst. Nanostruct.*, vol. 25, pp. 605–612, 2005.

[71] R. W. G. Wyckoff, *Crystal Structures*. New York: Interscience, 1968.

[72] P. Camagni, G. Faglia, P. Galinetto, C. Perego, G. Samoggia, and G. Sberveglieri, "Photosensitivity activation of SnO_2 thin film gas sensors at room temperature," *Sens. Actuators B*, vol. 31, pp. 99–103, 1996.

[73] N. Amin, T. Isaka, A. Yamada, and M. Konagai, "Highly efficient 1 mm thick CdTe solar cells with textured TCOs," *Solar Energy Mater. Solar Cells*, vol. 67, pp. 195–201, 2001.

[74] E. Comini, G. Faglia, and G. Sberveglieri, "UV light activation of tin oxide thin films for NO_2 sensing at low temperatures," *Sens. Actuators B*, vol. 78, pp. 73–77, 2001.

[75] A. A. Bolzan, C. Fong, B. J. Kennedy, and C. J. Howard, "Structural studies of rutile-type metal dioxides," *Acta Crystallogr. Sect. B, Struct. Sci.*, vol. 53, pp. 373–380, 1997.

[76] J. Tamaki, C. Naruo, Y. Yamamoto, and M. Matsuoka, "Sensing properties to dilute chlorine gas of indium oxide based thin film sensors prepared by electron beam evaporation," *Sens. Actuators B*, vol. 83, pp. 190–194, 2002.

[77] P. C. Chen, F. N. Ishikawa, and C. Zhou, "High performance transparent Indium oxide nanowire transistors," submitted for publication, 2007.

[78] S. Ju, K. Lee, M. Yoon, A. Facchetti, T. J. Marks, and D. B. Janes, "High performance ZnO nanowire field effect transistors with organic gate nanodielectrics: Effects of metal contacts and ozone treatment," *Nanotechnology*, vol. 18, pp. 155201-1–155201-7, 2007.

[79] B. Xiang, P. Wang, X. Zhang, S. A. Dayeh, D. P. R. Aplin, C. Soci, D. Yu, and D. Wang, "Rational synthesis of p-type zinc oxide nanowire arrays using simple chemical vapor deposition," *Nano Lett.*, vol. 7, pp. 323–326, 2007.

[80] G.-D. Yuan, W.-J. Zhang, J.-S. Jie, X. Fan, J.-X. Tang, I. Shafiq, Z.-Z. Ye, C.-S. Lee, and S.-T. Lee, "Tunable n-type conductivity and transport properties of Ga-doped ZnO nanowire array," *Adv. Mater.*, vol. 20, pp. 168–173, 2008.

[81] S. Ju, F. N. Ishikawa, P. Chen, H. Chang, and C. Zhou, "High performance In_2O_3 nanowire transistors using organic gate nanodielectrics," *Appl. Phys. Lett.*, vol. 92, pp. 222105–222107, 2008.

[82] S. Ju, P. Chen, C. Zhou, Y. Ha, A. Facchetti, T. M. Marks, S. K. Kim, S. Mohammadi, and D. B. Janes, "1/f noise of SnO_2 nanowire transistors," *Appl. Phys. Lett.*, vol. 92, pp. 243120–243122, 2008.

[83] E. N. Dattoli, Q. Wan, W. Guo, Y. Chen, X. Pan, and W. Lu, "Fully transparent thin-film transistor devices based on SnO_2 nanowires," *Nano Lett.*, vol. 7, pp. 2463–2469, 2007.

[84] J. M. Baik, M. H. Kim, C. Larson, X. Chen, S. Guo, A. M. Wodtke, and M. Moskovits, "High-yield TiO_2 nanowire synthesis and single nanowire field-effect transistor fabrication," *Appl. Phys. Lett.*, vol. 92, pp. 242111–242113, 2008.

[85] G. T. Kim, J. Muster, V. Krstic, J. G. Park, Y. W. Park, S. Roth, and M. Burghard, "Field-effect transistor made of individual V_2O_5 nanofibers," *Appl. Phys. Lett.*, vol. 76, pp. 1875–1877, 2000.

[86] P. Chang, Z. Fan, W. Tseng, A. Rajagopal, and J. G. Lu, "Beta-Ga_2O_3 nanowires: Synthesis, characterization, and p-channel field-effect transistor," *Appl. Phys. Lett.*, vol. 87, pp. 222102–222104, 2005.

[87] Z. Fan, X. Wen, S. Yang, and J. G. Lu, "Controlled p- and n-type doping of Fe_2O_3 nanobelt field effect transistors," *Appl. Phys. Lett.*, vol. 87, pp. 13113–13115, 2005.

[88] Y. Lee, Y. Chueh, C. Hsieh, M. Chang, L. Chou, Z. L. Wang, Y. Lan, C. Chen, H. Kurata, and S. Isoda, "p-Type alpha-Fe_2O_3 nanowires and their n-type transition in a reductive ambient," *Small*, vol. 3, pp. 1356–1361, 2007.

[89] B. Lei, C. Li, D. Zhang, T. Tang, and C. Zhou, "Tuning electronic properties of In_2O_3 nanowires by doping control," *Appl. Phys. A*, vol. 79, pp. 439–442, 2004.

[90] S. Ju, Y. Xuan, P. Ye, D. B. Janes, F. Ishikawa, C. Zhou, G. Lu, A. Facchetti, and T. J. Marks, "Fully transparent In_2O_3 and ZnO nanowire transistors," *Nature Nanotechnol.*, vol. 2, pp. 378–384, 2007.

[91] V. V. Sysoev, B. K. Button, K. Wepsoec, S. Dmitriev, and A. Kolmakov, "Toward the nanoscopic "electronic nose": Hydrogen vs. carbon monoxide discrimination with an array of individual metal oxide nano- and mesowire sensors," *Nano Lett.*, vol. 6, pp. 1584–1588, 2006.

[92] N. Barsan and U. Weimar, "Conduction model of metal oxide gas sensors," *J. Electroceram.*, vol. 7, pp. 143–167, 2001.

[93] S. Semancik and D. F. Cox, "Fundamental characterization of clean and gas-dosed tin oxide," *Sens. Actuators*, vol. 12, pp. 101–106, 1987.

[94] M. Batzill and U. Diebold, "The surface and materials science of tin oxide," *P. Surf. Sci.*, vol. 79, pp. 47–154, 2005.

[95] Z. Fan and J. G. Lu, "Gate-refreshable nanowire chemical sensors," *Appl. Phys. Lett.*, vol. 86, pp. 123510–123512, 2006.

[96] D. Zhang, C. Li, X. Liu, S. Han, T. Tang, and C. Zhou, "Dpoing dependent NH_3 sensing for indium oxide nanowires," *Appl. Phys. Lett.*, vol. 83, pp. 1845–1847, 2003.

[97] K. Ryu, D. Zhang, and C. Zhou, "High-performance metal oxide nanowire chemical sensors with integrated micromachined hotplates," *Appl. Phys. Lett.*, vol. 92, pp. 093111–093113, 2008.

[98] L. C. Tien, P. W. Sadik, D. P. Norton, L. F. Voss, S. J. Pearton, H. T. Wang, B. S. Kang, F. Ren, J. Jun, and J. Lin, "Hydrogen sensing at room temperature with Pt-coated ZnO thin films and nanorods," *Appl. Phys. Lett.*, vol. 87, pp. 222106–222108, 2005.

[99] E. S. Snow, F. K. Perkins, and J. A. Robinson, "Chemical vapor detection using single-walled carbon nanotubes," *Chem. Soc. Rev.*, vol. 35, pp. 790–798, 2006.

[100] D. Zhang, Z. Liu, C. Li, T. Tang, X. Liu, S. Han, B. Lei, and C. Zhou, "Detection of NO_2 down to ppb levels using individual and multiple In_2O_3 nanowire devices," *Nano Lett.*, vol. 4, pp. 1919–1924, 2004.

[101] C. S. Rout, M. Hegdge, and C. N. R. Rao, "H_2S sensors based on tungsten oxide nanostructures," *Sens. Actuators B*, vol. 128, pp. 488–493, 2008.

[102] J. Xu, Y. Chen, Y. Li, and J. Shen, "Gas sensing properties of ZnO nanorods prepared by hydrothermal method," *J. Mater. Sci.*, vol. 40, pp. 2919–2921, 2005.

[103] H. T. Wang, B. S. Kang, F. Ren, L. C. Tien, P. W. Sadik, D. P. Norton, S. J. Pearton, and J. Lin, "Hydrogen-selective sensing at room temperature with ZnO nanorods," *Appl. Phys. Lett.*, vol. 86, pp. 243503–243505, 2005.

[104] C. Wang, X. Chu, and M. Wu, "Detection of H_2S down to ppb levels at room temperature using sensors based on ZnO nanorods," *Sens. Actuators B*, vol. 113, pp. 320–323, 2006.

[105] G. Sberveglieri, C. Baratto, E. Comini, G. Faglia, M. Ferroni, A. Ponzoni, and A. Vomiero, "Synthesis and characterization of semiconducting nanowires for gas sensing," *Sens. Actuators B*, vol. 121, pp. 208–213, 2007.

[106] Q. Wan, Q. H. Li, Y. J. Chen, T. H. Wang, X. L. He, J. P. Li, and C. L. Lin, "Fabrication and ethanol sensing characteristics of ZnO nanowire gas sensors," *Appl. Phys. Lett.*, vol. 84, pp. 3654–3656, 2004.

[107] P. Xu, Z. Cheng, Q. Pan, J. Xu, Q. Xiang, W. Yu, and Y. Chu, "High aspect ratio In_2O_3 nanowires: Synthesis, mechanism and NO_2 gas-sensing properties," *Sens. Actuators B*, vol. 130, pp. 802–808, 2008.

[108] A. Vomiero, S. Bianchi, E. Comini, G. Faglia, M. Ferroni, and G. Sberveglieri, "Controlled growth and sensing properties of In_2O_3 nanowires," *Crystal Growth Des.*, vol. 7, pp. 2500–2504, 2007.

[109] N. Du, H. Zhang, B. Chen, X. Ma, Z. Liu, J. Wu, and D. Yang, "Porous indium oxide nanotubes: Layer-by-layer assembly on carbon-nanotube templates and application for room-temperature NH_3 gas sensors," *Adv. Mater.*, vol. 19, pp. 1641–1645, 2007.

[110] L. Francioso, A. M. Taurino, A. Forleo, and P. Siciliano, "TiO_2 nanowires array fabrication and gas sensing properties," *Sens. Actuators B*, vol. 130, pp. 70–76, 2008.
[111] Y. Wang, G. Du, H. Liu, D. Liu, S. Qin, N. Wang, C. Hu, X. Tao, J. Jiao, J. Wang, and Z. L. Wang, "Nanostructured sheets of Ti–O nanobelts for gas sensing and antibacterial applications," *Adv. Funct. Mater.*, vol. 18, pp. 1131–1137, 2008.
[112] O. K. Varghese, D. Gong, M. Paulose, K. G. Ong, and C. A. Grimes, "Hydrogen sensing using titania nanotubes," *Sens. Actuators B*, vol. 93, pp. 338–344, 2003.
[113] I. D. Kim, A. Rothschild, B. H. Lee, D. Y. Kim, S. M. Jo, and H. L. Tuller, "Ultrasensitive chemiresistors based on electrospun TiO_2 nanofibers," *Nano Lett.*, vol. 6, pp. 2009–2013, 2006.
[114] D. C. Meier, S. Semancik, B. Button, E. Strelcov, and A. Kolmakov, "Coupling nanowire chemiresistors with MEMS microhotplate gas sensing platforms," *Appl. Phys. Lett.*, vol. 91, pp. 63118–63120, 2007.
[115] F. Hernández-Ramírez, A. Tarancón, O. Casals, J. Arbiol, A. Romano-Rodríguez, and J. R. Morante, "High response and stability in CO and humidity measures using a single SnO_2 nanowire," *Sens. Actuators B*, vol. 121, pp. 3–17, 2007.
[116] M. Law, H. Kind, B. Messer, F. Kim, and P. Yang, "Photochemical sensing of NO_2 with SnO_2 nanoribbon nanosensors at room temperature," *Angew. Chem. Int. Ed.*, vol. 41, pp. 2405–2408, 2002.
[117] G. X. Wang, J. S. Park, M. S. Park, and X. L. Gou, "Synthesis and high gas sensitivity of tin oxide nanotubes," *Sens. Actuators B*, vol. 131, pp. 313–317, 2008.
[118] Y. J. Chen, L. Nie, X. Y. Xue, Y. G. Wang, and T. H. Wang, "Linear ethanol sensing of SnO_2 nanorods with extremely high sensitivity," *Appl. Phys. Lett.*, vol. 88, pp. 83105–83107, 2006.
[119] Z. Ying, Q. Wan, Z. T. Song, and S. L. Feng, "SnO_2 nanowhiskers and their ethanol sensing characteristics," *Nanotechnology*, vol. 15, pp. 1682–1684, 2004.
[120] Y. Zhang, X. Ha, J. Li, Z. Miao, and F. Huang, "Fabrication and ethanol-sensing properties of micro gas sensor based on electrospun SnO_2 nanofibers," *Sens. Actuators B*, vol. 132, pp. 67–73, 2008.
[121] X. Y. Xue, Y. J. Chen, Y. G. Liu, S. L. Shi, Y. G. Wang, and T. H. Wang, "Synthesis and ethanol sensing properties of indium-doped thin oxide nanowires," *Appl. Phys. Lett.*, vol. 88, pp. 201907–201909, 2006.
[122] Q. Wan, J. Huang, Z. Xie, T. Wang, E. N. Dattoli, and W. Lu, "Branched SnO_2 nanowires on metallic nanowire backbones for ethanol sensors application," *Appl. Phys. Lett.*, vol. 92, pp. 102101–102103, 2008.
[123] L. H. Qian, K. Wang, Y. Li, H. T. Fang, Q. H. Lu, and X. L. Ma, "CO sensor based on Au-decorated SnO_2 nanobelt," *Mater. Chem. Phys.*, vol. 100, pp. 82–84, 2006.
[124] J. Liu, X. Wang, Q. Peng, and Y. Li, "Vanadium pentoxide nanobelts: Highly selective and stable ethanol sensor materials," *Adv. Mater.*, vol. 17, pp. 764–767, 2005.
[125] I. Raible, M. Burghard, U. Schlecht, A. Yasuda, and T. Vossmeyer, "V_2O_5 nanofibers: Novel gas sensors with extremely high sensitivity and selectivity to amines," *Sens. Actuators B*, vol. 106, pp. 730–735, 2005.
[126] L. C. Short and T. Benter, "Selective measurement of HCHO in urine using direct liquid-phase fluorimetric analysis," *Clin. Chem. Lab. Med.*, vol. 43, pp. 178–182, 2005.
[127] S. Sze, *Physics of Semiconductor Devices*. New York: Wiley, 1981.
[128] C. Zhou, J. Kong, E. Yenilmez, and H. Dai, "Modulated chemical doping of individual carbon nanotubes," *Science*, vol. 290, pp. 1552–1555, 2000.
[129] B. Panchapakesan, R. Cavicchi, S. Semancik, and D. L. DeVoe, "Sensitivity, selectivity and stability of tin oxide nanostructures on large area arrays of microhotplates," *Nanotechnology*, vol. 17, pp. 415–425, 2006.
[130] T. G. G. Maffeis, G. T. Owen, M. W. Penny, T. K. H. Starke, S. A. Clark, H. Ferkel, and S. P. Wilks, "Nano-crystalline SnO_2 gas sensor response to O-2 and CH_4 at elevated temperature investigated by XPS," *Surf. Sci.*, vol. 520, pp. 29–34, 2002.
[131] A. Helwig, G. Muller, G. Sberveglieri, and G. Faglia, "Gas response times of nano-scale SnO_2 gas sensors as determined by the moving gas outlet technique," *Sens. Actuators B*, vol. 126, pp. 174–180, 2007.
[132] X. H. Chen and M. Moskovits, "Observing catalysis through the agency of the participating electrons: Surface-chemistry-induced current changes in a tin oxide nanowire decorated with silver," *Nano Lett.*, vol. 7, pp. 807–812, 2007.
[133] W. P. Tai and J. H. Oh, "Fabrication and humidity sensing properties of nanostructured TiO_2–SnO_2 thin films," *Sens. Actuators B*, vol. 85, pp. 154–157, 2002.
[134] X. Gou, G. Wang, J. Yang, J. Park, and D. Wexler, "Chemical synthesis, characterization and gas sensing performance of copper oxide nanoribbons," *J. Mater. Chem.*, vol. 18, pp. 965–969, 2008.
[135] C. Wang, X. Q. Fu, X. Y. Xue, Y. G. Wang, and T. H. Wang, "Surface accumulation conduction controlled sensing characteristic of p-type CuO nanorods induced by oxygen adsorption," *Nanotechnology*, vol. 18, pp. 145506–145510, 2007.
[136] J. Polleux, A. Gurlo, N. Barsan, U. Weimar, M. Antonietti, and M. Niederberger, "Template-free synthesis and assembly of single-crystalline tungsten oxide nanowires and their gas-sensing properties," *Angew. Chem. Int. Ed.*, vol. 45, pp. 261–265, 2006.
[137] C. S. Rout, K. Ganesh, A. Govindaraj, and C. N. R. Rao, "Sensors for the nitrogen oxides, NO_2, NO, and N_2O, based on In_2O_3 and WO_3 nanowires," *Appl. Phys. A*, vol. 85, pp. 241–246, 2006.
[138] Y. S. Kim, S. C. Ha, and K. Kim, "Room-temperature semiconductor gas sensor based on nonstoichiometric tungsten oxide nanorod film," *Appl. Phys. Lett.*, vol. 86, pp. 213105-1–213105-3, 2005.
[139] M. A. Craven, J. W. Gardner, and P. N. Bartlett, "Electronic noses—Development and future prospects," *Trends Anal. Chem.*, vol. 15, pp. 486–493, 1996.
[140] K. Persaud and G. H. Dodd, "Analysis of discrimination mechanisms of the mammalian olfactory system using a model nose," *Nature*, vol. 299, pp. 352–355, 1982.
[141] Y. Lu, C. Partridge, M. Meyyappan, and J. Li, "A carbon nanotube sensor array for sensitive gas discrimination using principal component analysis," *J. Electroanal. Chem.*, vol. 593, pp. 105–110, 2006.
[142] M. C. McApline, H. Ahmad, D. Wang, and J. R. Heath, "Highly ordered nanowire arrays on plastic substrates for ultrasensitive flexible chemical sensors," *Nature Mater.*, vol. 6, pp. 1–6, 2007.
[143] P. Althainz, A. Dahlke, M. Frietsch-Klarhof, J. Goschnick, and H. J. Ache, "Reception tuning of gas-sensor microsystem by selective coating," *Sens. Actuators B*, vol. 24/25, pp. 366–369, 1995.
[144] J. Folch, X. G. Capdevila, M. Segarra, and J. R. Morante, "Solid electrolyte multisensor system for detecting O_2, CO, and NO_2," *J. Electrochem. Soc.*, vol. 154, pp. J201–J208, 2007.
[145] P. T. Moseley, "New trends and future prospects of thick- and thin-film gas sensors," *Sens. Actuators B*, vol. 3, pp. 167–174, 1991.
[146] D. Then, A. Vidic, and C. H. Ziegler, "A highly sensitive self-oscillating cantilever array for the quantitative and qualitative analysis of organic vapor mixtures," *Sens. Actuators B*, vol. 117, pp. 1–9, 2006.
[147] P. C. Chen, F. N. Ishikawa, H. K. Chang, K. Ryu, and C. Zhou, "Nano electronic nose: A hybrid nanowire/carbon nanotube sensor array with integrated micromachined hotplates for sensitive gas discrimination," submitted for publication.
[148] P. Althainz and J. Goschnick, "Sensor for reducing or oxidizing gases," U.S. Patent 5 783 154, 1998.
[149] C. Arnold, M. Harms, and J. Goschnick, "Air quality monitoring and fire detection with the Karlsruhe electronic micronose KAMINA," *IEEE Sens. J.*, vol. 2, no. 3, pp. 179–188, Jun. 2002.
[150] V. V. Sysoev, I. Kiselev, M. Frietsch, and J. Goschnick, "Temperature gradient effect on gas discrimination power of a metal-oxide thin-film sensor microarray," *Sensors*, vol. 4, pp. 37–46, 2004.
[151] J. Goschnick, I. Koronczi, M. Frietsch, and I. Kiselev, "Water pollution recognition with the electronic nose KAMINA," *Sens. Actuators B*, vol. 106, pp. 182–186, 2005.
[152] V. V. Sysoev, J. Goschnick, T. Schneider, E. Strelcov, and A. Kolmakov, "A gradient microarray electronic nose based on percolating SnO_2 nanowire sensing elements," *Nano Lett.*, vol. 7, pp. 3182–3188, 2007.

Po-Chiang Chen received the B.S. degree in physics from Tamkang University, Taipei, Taiwan, in 1999, and the M.S. degree in optoelectronics from the National Taipei University of Technology, Taipei, in 2001. He is currently working toward the Ph.D. degree in chemical engineering and materials science at the University of Southern California, Los Angeles.

His current research interests include the device applications based on 1-D nanomaterials, including chemical sensors, transparent electronics, and energy conversion and storage devices.

Guozhen Shen received the B.S. degree in chemical education from Anhui Normal University, Wuhu, China, in 1999, and the Ph.D. degree in chemistry from the University of Science and Technology of China, Hefei, China, in 2003.

He was a Postdoctoral Researcher at Hanyang University, Korea, in 2004. He then joined the National Institute for Materials Science, Japan, as a Visiting Researcher. He is currently a Research Scientist at the University of Southern California, Los Angeles. He is the author or coauthor of more than 90 research articles, five book chapters, and several patents. His current research interests include the synthesis and characterization of 1-D nanostructures and their device application in electronics and optoelectronics.

Chongwu Zhou received the B.S. degree from the University of Science and Technology of China, Hefei, China, in 1993 and the Ph.D. degree in electrical engineering from Yale University, New Haven, CT, in 1999.

He was a Postdoctoral Research Fellow at Stanford University from November 1998 to June 2000. In September 2000, he joined the University of Southern California (USC), Los Angeles. His research group has been working at the forefront of nanoscience and nanotechnology, including synthesis and applications of carbon nanotubes and nanowires, biosensing, and nanotherapy.

Dr. Zhou has won a number of awards, including the National Science Foundation (NSF) CAREER Award, the National Aeronautics and Space Administration (NASA) Turning Goals Into Reality (TGiR) Award, the USC Junior Faculty Research Award, and the IEEE Nanotechnology Early Career Award. He is currently an Associate Editor for the IEEE TRANSACTIONS ON NANOTECHNOLOGY.